Dynamic Intensity Borrowing in Porphyrin J-Aggregates Revealed by Sub-5-fs Spectroscopy

Hideaki Kano, Takashi Saito, and Takayoshi Kobayashi*

Department of Physics, University of Tokyo, Hongo 7-3-1, Bunkyo, Tokyo 113-0033, Japan

Received: July 24, 2000; In Final Form: October 27, 2000

Sub-5-fs spectroscopy of porphyrin J-aggregates reveals a coherent molecular vibration coupled to the Frenkel exciton. The bleaching and induced absorption signals show synchronous oscillations with the frequency of 244 cm^{-1}. The coherent oscillation is explained by a modulated transition dipole moment, which is due to a dynamic intensity borrowing from the intense B-transition to the weak Q-transition through the ruffling mode with the 244 cm^{-1}-frequency.

Introduction

Molecular J-aggregates have attracted much attention because of their several characteristic features of their spectroscopic properties.[1−3] Intermolecular interaction between transition dipole moments results in the coherent delocalization of excitons over an aggregate.[2] Recently it was found that the aggregate has a hierarchical structure, which is described by a macroaggregate composed of many mesoaggregates.[4] The aggregation forces in the former and latter are due to the van der Waals interaction and static dipole−dipole ($\mu_{st}-\mu_{st}$) interaction. The transition-dipole−transition dipole ($\mu_{tr}-\mu_{tr}$) interaction suffers much from thermal fluctuation because of weaker long-range dependence ($1/r^6$) than the static dipole−dipole interaction ($1/r^3$). The thermal fluctuation of the order of phonons in the aggregate system with the wavelength λ_{ph} disturbs the $\mu_{tr}-\mu_{tr}$ interaction, but it does not deteriorate the $\mu_{tr}-\mu_{tr}$ interaction. The growth of the mesoaggregate stops at the aggregate size of $r \approx (kT/\mu_{tr}^2)^{1/3}$, where kT is the thermal energy. The mesoaggregates then have a large static dipole moment accumulated, and further aggregation of mesoaggregates forms a macroaggregate, since the former is not much disturbed by the thermal fluctuation up to the size level of $r \approx (kT/\mu_{st}^2)^{1/3}$. It is very important to well characterize the above hierarchical structure to discuss the experimental results obtained by coherent interaction with a coherent laser pulse. Hereafter the name "J-aggregate" is used for a mesoaggregate.

The excitonic transition of the J-aggregates is characterized by a sharp absorption band, called the J-band, of which the transition energy is lower than that of monomers by twice the dipole−dipole interaction, J.[5,6] Among J-aggregates composed of various aromatic or macrocyclic compounds, tetraphenylporphine tetrasulfonic acid (TPPS) J-aggregates are of special interest since they are model substances for aggregates of the light-harvesting antenna chlorophyll with a storage ring configuration and of primary charge-separation systems in photosynthesis. Since the first studies of the formation of the J-aggregates independently reported by Fleischer et al.[7] and Pasternack et al.,[8] a number of investigations have been performed using linear and nonlinear electronic spectroscopies which elucidated the optical properties characteristic of the excitonic transition in porphyrin J-aggregates.[9−17] The absorption spectrum of TPPS aggregates shows a relatively weak band in the visible region and a strong peak in the near-ultraviolet, denoted as Q- and B-bands, respectively, composing a two-band Frenkel exciton system. Especially it is noted that a stationary fluorescence of the J-aggregates shows a small Stokes shift (∼20 meV). Although several studies have been made of exciton−phonon coupling,[18−20] few investigations related to the coherent molecular vibration coupled to the exciton in J-aggregates have been reported[21] in real time domain because the excitons interact only weakly with vibrations and very high time resolution is required for direct measurement of intramolecular vibrations. Recent progress of ultrashort laser pulses enables us to investigate directly the coherent molecular vibration induced by the electronic transition. Since wave packet motions in dye molecules and bacteriorhodopsin were reported by Shank and co-workers,[22−24] various materials in the condensed phase, including the chlorophyll J-aggregates,[21] have been studied by real-time spectroscopy.[25−31] Recently, we developed a novel optical parametric amplifier (OPA) which generates sub-5-fs visible pulses.[30,32] The parametric amplifier is in the noncollinear geometry with the pump pulse in a pulse-front tilting configuration. The noncollinear optical parametric amplifier (NOPA) has also two sets of chirped mirrors to compensate for the group velocity dispersion between the signal and idler before and after the OPA. In the present study, we apply the sub-5-fs real-time spectroscopy to study the exciton-vibration coupling in the one-dimensional Frenkel exciton system. The coherent molecular vibration is clearly observed in the time dependence of the transmission change. The experimental results are well explained by a new model, modulated Q-band−transition dipole moment, which originates from the oscillator strength transfer from the intense B-band to the weak Q-band by dynamic intensity borrowing (DIB) mechanism through the vibronic interaction.

Experimental Section

Sample Preparation. Tetraphenylporphine tetrasulfonic acid (TPPS; Tokyo Kasei) and poly(vinyl alcohol) (PVA; Kanto Chemical) were used without further purification. After 200 mg of PVA was dissolved into 4 mL of distilled water at ∼100 °C, 20 mg of TPPS was added into the hot solution. The concentration of TPPS was 5×10^{-3} mol/L, which is high enough for aggregate formation. A unidirectionally oriented film of porphyrin J-aggregates was prepared using a vertical spin-coating technique developed previously by our group.[33] Figure 1 shows linear absorption spectra of porphyrin J-aggregates and monomer. Sharp absorption peaks at 2.53 eV (S_2-state; B_x-band or

* Corresponding author. E-mail: kobayashi@phys.s.u-tokyo.ac.jp.

10.1021/jp0026134 CCC: $20.00
Published on Web 12/22/2000

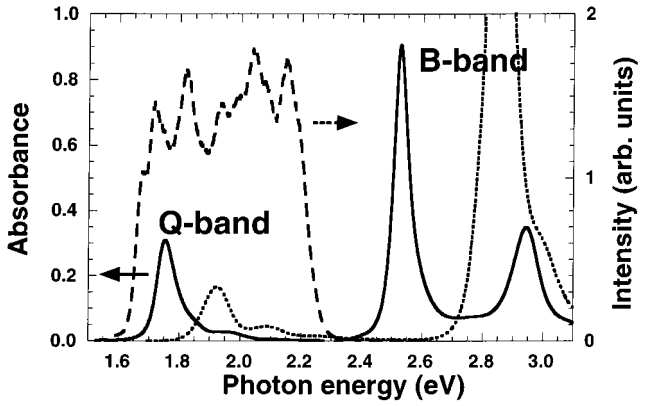

Figure 1. Linear absorption spectra of porphyrin J-aggregates (solid line) and monomer (dotted line). The dashed line shows the laser spectrum.

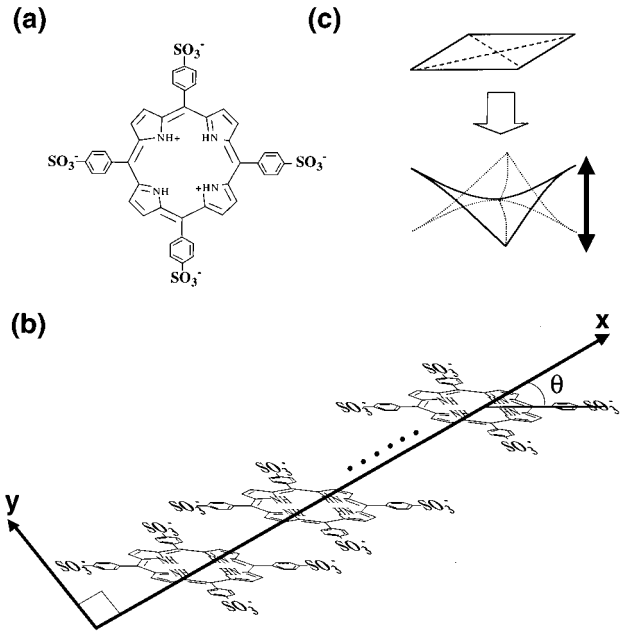

Figure 2. Structures of a porphyrin molecule (a) and J-aggregate (b). The *x* axis corresponds to a stacking direction. The porphyrin molecules make an angle θ with the *x* axis. (c) Structural diagram of the ruffling motion of the porphyrin molecule.

Soret band) and 1.75 eV (S_1-state; Q_x-band) correspond to B- and Q-exciton bands, respectively, composing a quasi-two-band Frenkel-exciton system. Both B_x- and Q_x-bands are positioned at lower energy side of those of the monomer (2.86 and 1.92 eV). The latter and former correspond to the lowest and second lowest singlet excited states (S_1- and S_2-states), respectively. Fine structures in the absorption bands indicate counterparts of the two bands, namely, the B_y- and Q_y-bands, which have peaks around 2.94 and 1.86 eV, respectively. Because of the polarization dependence of the absorption, it can be stated that the *x* and *y* components originate from the transition dipole moments which are parallel and perpendicular, respectively, to the aggregate axis defined as a direction connecting the centers of neighboring molecules composing an aggregate. The *x* and *y* components are assigned to J-type and H-type aggregates.[11] The structure of the TPPS aggregate is shown in Figure 2.[13,14,16] A component of the aggregate is a protonated TPPS molecule, which has a nearly coplanar structure between the phenyl rings and the porphyrin ring. As is shown in Figure 2, the porphyrins are stacked, but the sulfonic group of one TPPS unit is directly above the diacid charge of another, which contributes to the stability of the aggregate.

Real-Time Pump−Probe Experimental Apparatus. The experimental setup of the sub-5-fs time-resolved pump−probe system is based on the lock-in detection and is described elsewhere.[28] Here only the important parameters of the experimental system are described. The probe pulse intensity after the sample is spectrally dispersed by a 30 cm monochoromator (Ritsu, MC-30) and measured with a Si photodiode. The spectral resolution of the whole system is about 3 nm. The broad spectrum of the probe pulse enables the investigation over the wide spectral range from 1.6 to 2.3 eV. All measurements are performed at room temperature. Although the pulse duration is shorter than 5 fs, the fwhm of the cross-correlation trace is broadened to about 8 fs because of the geometrical smearing due to a finite angle between the pump and probe beams to avoid an artificial signal caused by the interference between them. The pump pulse energy and photon density are about 14 nJ and 5.9×10^{14} photons/cm^2, respectively. Both the polarizations of the pump and probe are parallel to the aggregate axis (*x*-axis).

Results and Discussion

Real-Time Spectra. The time dependence of the transmittance change in porphyrin J-aggregates at seven different probe photon energies is shown in Figure 3a. The laser spectrum covers the whole width of the Q-band of the TPPS J-aggregates, while the B-band is outside of the laser spectrum. It can be safely assumed that the Q-exciton is created by the one-photon resonant transition process and no B-exciton can be produced at the excitation photon flux of 1.2×10^{29} photons/s·cm^2. The predominant feature commonly found in the traces is high-frequency oscillations in addition to the underlying slow-dynamics transient components. The oscillation period is 137 $\pm$ 4 fs and the oscillations persist for delay times longer than 1 ps. As will be discussed in detail, the phase of the transient oscillation is reversed between the bleaching and induced absorption, which is clearly shown in Figure 4. Because of the sub-10-temporal resolution, the phases of the oscillation are precisely determined to be -0.3 ± 0.1 and -0.3 ± 0.1 radian at 1.72 and 1.80 eV, respectively, using a cosine function. The oscillation at $E_{probe} < 1.77$ eV is described by a plus-cosine function, whereas the oscillation at $E_{probe} > 1.77$ eV is expressed by a minus-cosine function. The oscillatory signal size is drastically reduced around 1.77 eV.

The overall slow dynamics of the transmittance change originates from the dynamics of the excited states of J-aggregates by photoexcitation. The positive signal observed over the whole range of delay times for $E_{probe} < 1.77$ eV is attributed to a bleaching between the Q-band and the ground state. At probe energies higher than 1.8 eV, the signal becomes negative due to an induced absorption (IA). Additional complex oscillating features observed both at a negative delay and around the time origin are due to the pump-perturbed free induction decay[34] and to cross-phase modulation,[35] and are also partly due to the interference left over between the pump and probe pulses. Measured decay curves of the transmittance change are fitted by the sum of two exponential-decay functions, which is convoluted with the cross-correlation function. Since nearly chirp-free pulses are used for both pump and probe, the same cross-correlation function can be used for convolution with the response function over the whole range of the probe-photon energy. At the peak of the Q-band ($E_{probe} = 1.75$ eV), the fast and slow decay components are determined to be 45 $\pm$ 4 fs and 1.5 $\pm$ 0.1 ps, respectively.

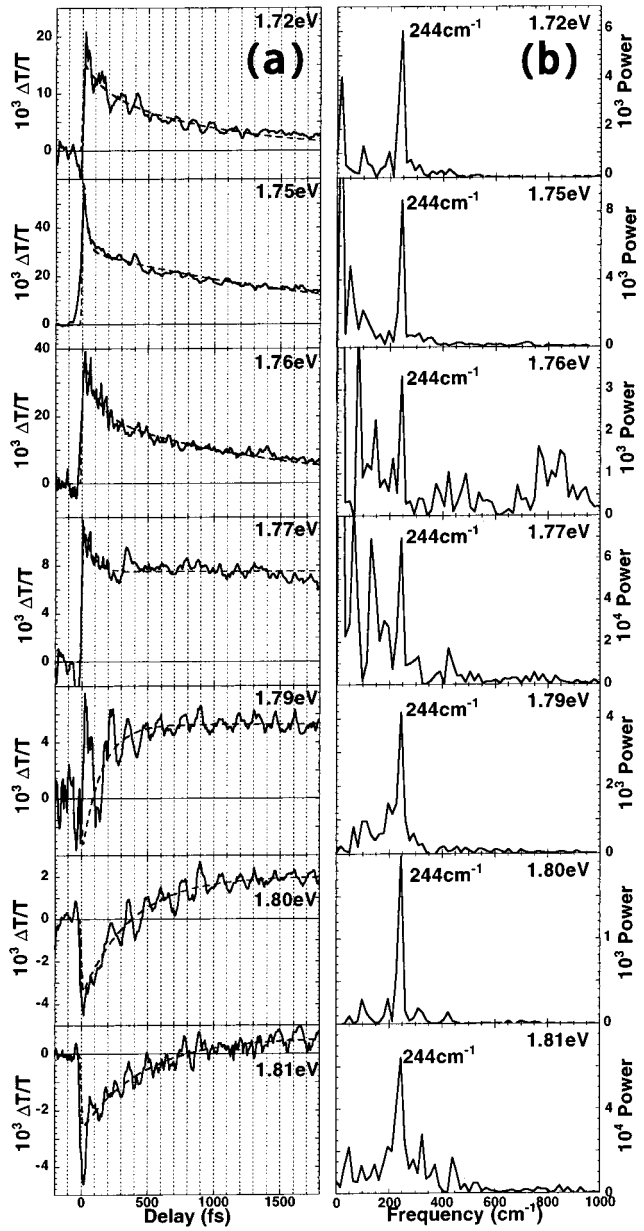

Figure 3. (a) Time dependence of the transmittance change in porphyrin J-aggregates at seven photon energies marked on the right. (b) Fourier power spectra of real-time spectra integrated from 100 fs to 1.8 ps.

Dynamics of the Excitonic States. The time-dependent transmittance change is composed of the excitonic and molecular vibrational contributions. The former and the latter correspond to the slow-dynamics component and the oscillating component, respectively. It is noteworthy that the oscillating component is observed only around the Q-band. In this subsection, we shall focus on the slow-dynamics component. The signal is composed of three components, namely the bleaching due to $|1,S_1\rangle \rightarrow |G\rangle$, IA due to the transition to multiexciton states (MES; $|n+1,S_1\rangle \leftarrow |n,S_1\rangle$ ($n = 1, 2, ...$)), and IA due to the transition to higher excited exciton states ($|1,S_n\rangle \leftarrow |n,S_1\rangle$ ($n = 2, 3, ...$)). Here n in $|n,S_1\rangle$ denotes the number of the S_1-excitons (Q-excitons) in a single mesoaggregate,[36−38] and $|1,S_n\rangle$ indicates one-exciton state of S_n-exciton, namely the excited state of an exciton originated from an S_n-excited state in a TPPS molecule. Although both the induced emission ($|1,S_1\rangle \rightarrow |G\rangle$) and ground-state depopulation ($|1,S_1\rangle \leftarrow |G\rangle$) can contribute to the bleaching signal, the former is considered to be a dominant effect for the oscillation.

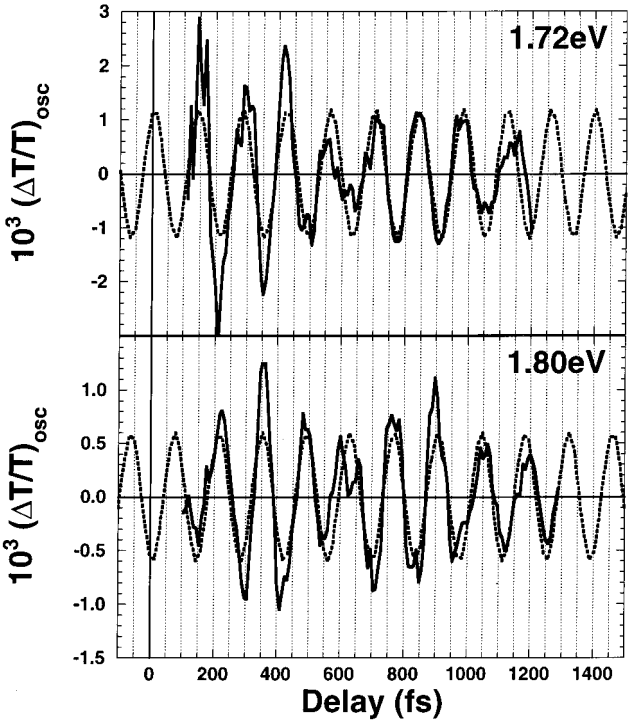

Figure 4. Oscillating component at two probe-photon energies (solid line) and results of the fitting using a cosine function (dashed line). Note that the phases are reversed with each other.

This is because the oscillatory signal due to the latter, which corresponds to the impulsive stimulated Raman scattering, must be described by a sine function.

The positive signal in the difference transmittance $\Delta T/T(t)$ around the Q-band is associated with the bleaching, while the negative signal originates from two sources. First, the IA with the transient oscillation is observed only around the Q-band. Since the IA due to the transition to MES should be observed at the probe-photon energy higher than the peak photon energy in the stationary absorption spectrum due to Pauli exclusion principle, the IA with the transient oscillation is attributable to the IA due to the transition to MES. The existence of the transition to MES is also confirmed by a study of a time-resolved pump−probe experiment using 100-fs-pump pulse.[39] Second, the IA without the transient oscillation has a broad spectrum far above the Q-band. It is ascribed to the IA due to the transition to the higher excited exciton states, because the absorption spectra of S_n-exciton states ($n \gg 1$) are expected to be broad and the oscillation is smeared.

Next we shall focus on the origin of the slow and fast decay components. The lifetime of the Q-exciton is reported to be ∼100 ps.[14,16,17] Hence, both the slow and fast decay components cannot be attributable to the Q-exciton lifetime. In our previous study, the decay time constant of the 1-ps component increased with the excitation power and the signal amplitude was superlinearly dependent on the pump power.[17] From these results, it was attributed to the lifetime of the S_2-exciton photogenerated by two-photon absorption. In our more recent report, however, it was found that the spectrum of the 1-ps component in IA shifted to the blue side as the delay time increased in the pump−probe experiment using a 100-fs-pump pulse.[39] Similar behavior is also observed in the IA ($|1,S_n\rangle \leftarrow |1,S_1\rangle$ ($n = 2, 3, ...$)) signal in the present experiment. Figure 5 shows the probe-photon energy dependence of the decay time constants of the slow and fast decay components. The slow decay time constant of IA

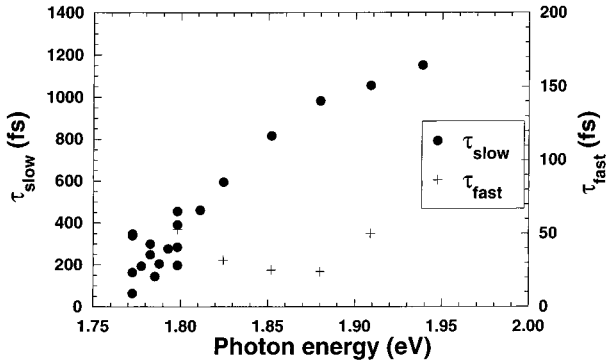

Figure 5. Probe-photon energy dependence of the slow (τ_{slow}) and fast (τ_{fast}) decay time constants in transient signals.

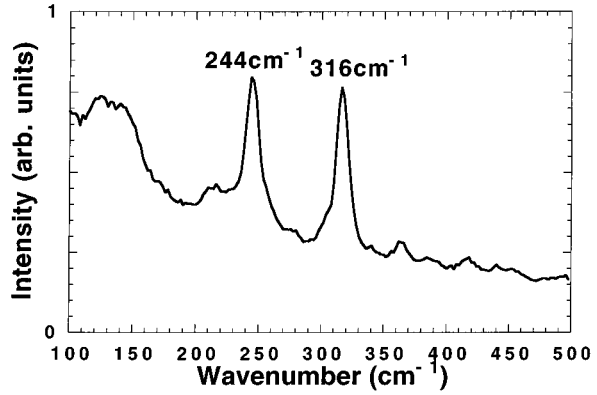

Figure 6. Resonance Raman spectrum of porphyrin J-aggregates. The excitation wavelength corresponds to 488 nm.

increases up to 1.2 ps with probe-photon energy, which means blue-shifted IA. These results indicate that the slow decay component cannot be attributable to the two-photon generated S_2-exciton. This component is, therefore, ascribed to the nonthermal S_1-excitons (Q-excitons) which thermalize with time constant of about 1 ps. In fact, the slow decay time constant increases slightly with the pump power in ref 17, which also supports this assignment. On the other hand, the decay time constant of the fast decay component is insensitive to the probe-photon energy and the time constant is about 100 fs. This component is attributable to the fast relaxation process from higher MESs ($|n+1,S_1\rangle \leftarrow |n,S_1\rangle$ (n = 1, 2, ...)), which is expected to be faster than the recovery of the bleaching. In the following, the bleaching and IA ($|n+1,S_1\rangle \leftarrow |n,S_1\rangle$ (n = 1, 2, ...)) signals with transient oscillation will be considered.

Analysis of the Coherent Molecular Vibration. For the discussion of the molecular vibration, the oscillating component must be separated from the transient curves. The result of the fitting of the slow-dynamics decay component is subtracted from the transient signal and only the oscillating component can be extracted. Figure 3b shows the Fourier-power spectra calculated from the oscillating components. The resolution is determined to be 16 cm^{-1} (fwhm) by the width of the delay-time window (1.7 ps) in the Fourier transformation analysis. The Fourier spectra clearly show an intense peak at 244 ± 8 cm^{-1}, which corresponds to a 137 ± 4 fs oscillation period in the whole spectral region of the Q-band. The intensity of the Fourier spectrum at 244 cm^{-1} is drastically reduced around 1.77 eV, near which the sign of the amplitude is changed.

The resonance Raman experiment is also performed for the same sample under the excitation of the B-band, which is shown in Figure 6. The peak at 244 cm^{-1} is clearly observed, which corresponds to the frequency obtained by the sub-5-fs real-time

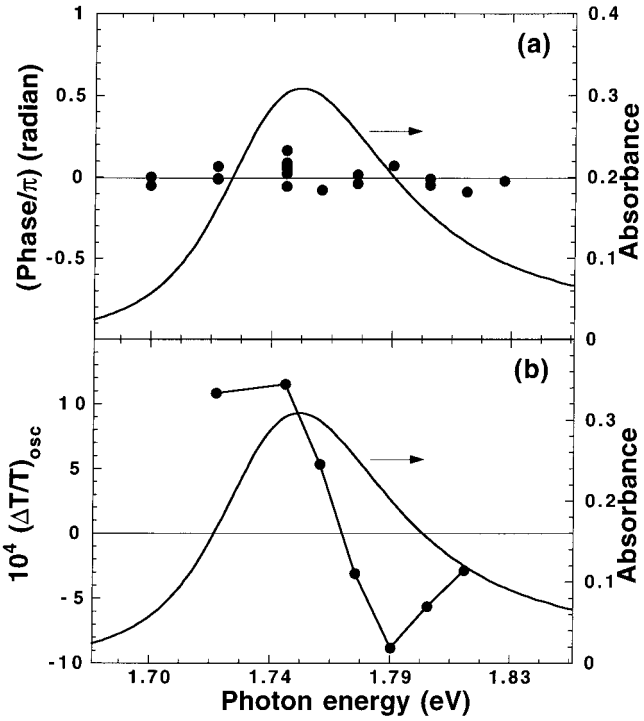

Figure 7. Probe-photon energy dependence of the phase (a) and amplitude (b) of the oscillation in the transient signals.

spectroscopy. The frequency of this peak is also detected at 245 cm^{-1} [11] and 241 cm^{-1} [14] in the stationary Raman spectrum. This peak is assigned to a ruffling mode, which is more than 30 times enhanced by aggregation[14] because the change in the molecular configuration associated with the vibrational mode is expected to strongly influence the dipole−dipole interaction. The ruffling motion is one of the out-of-plane modes, which is defined by four alternate up- or down-positioned nitrogen atoms with respect to the average plane of the macrocycle (Figure 2(c)).[14] The 316 cm^{-1} doming mode, which is another aggregation-enhanced intense Raman mode in the stationary Raman spectrum, is not observed in the real-time spectra. Note that both modes are observed in the Raman scattering experiment under resonant excitation of the B-band. On the other hand, our experiment of the sub-5-fs real-time spectroscopy is performed under resonant excitation of the Q-band. The ratio of the 244 cm^{-1}-ruffling mode to the 316 cm^{-1} doming mode may depend on the excitation photon energy and the detection method. It is also of interest to study experimentally the stationary resonance Raman spectrum under the Q-band resonance condition.

Next, the phase of the oscillation is evaluated by the complex Fourier transformation. Figure 7 shows the probe photon energy dependence of the phase and amplitude of the 244 cm^{-1} ruffling mode. As was shown previously in Figure 4, the oscillations are described by a plus-cosine or a minus-cosine function at $E_{probe} < 1.77$ eV or $E_{probe} > 1.77$ eV, respectively, indicating that the sign of the amplitude is reversed around 1.77 eV. Around 1.77 eV, the transient signal itself changes from the bleaching (positive signal) to the IA (negative signal) and the oscillation amplitude is extremely decreased. The plus-cosine oscillation in the bleaching and the minus-cosine oscillation in the IA indicate that the bleaching and IA increase (or decrease) synchronously (in-phase oscillation).

Several reports based on numerical calculation on the transmittance change in medium-size molecules photoexcited by an ultrashort pulse have attributed the transient oscillation

to the dynamics of localized vibrational wave packets which move on the electronic ground or excited potential energy surfaces.[22−24] In these cases, the phase of the transient oscillation is expected to be shifted continuously by changing the probe-photon energy, because the transition energy depends on the nuclear position, and different photon energies of the probe pulse are absorbed at different nuclear positions. Based on the conventional wave packet motion on a harmonic potential of the vibronic excited state, we estimate the probe photon energy dependence of the phase of the oscillation. The phase of the transient oscillation must show π-phase difference between $E_{probe} = E_{abs} = 1.75$ eV and $E_{probe} = 2E_{fluo} - E_{abs} = 1.71$ eV, where E_{abs} and E_{fluo} correspond to the peak photon energies of the absorption and fluorescence spectra, respectively. Although it is well resolved in the present experiment ($\sim$0.01 eV), the π-phase difference is not observed. In addition to this, it is well-known that the J-band associated with excitonic transition in J-aggregates interacts only weakly with molecular vibrations, which is a manifestation of the small Stokes shift in the stationary fluorescence spectrum. These results indicate that the vibronic coupling is much smaller than in the typical medium-size molecules such as Nile blue.[22,23] Because of these reasons, the oscillation does not originate from conventional vibronic coupling between the excitonic transition and relevant molecular vibrations represented by the wave packet motion. Since the signal intensities of the bleaching and IA vary synchronously, and the oscillation is observed only around the Q-band, we propose a new mechanism which also induces the transient oscillation: the modulated transition dipole moment of the Q-transition in the TPPS molecules. The modulation frequency corresponds to the 244 cm^{-1} ruffling mode vibration. Since the transition dipole moment depends on the normal vibrational coordinate, it means that this model is beyond Condon approximation. The increase (or decrease) in the transition dipole moment is reflected by the increase (or decrease) in the signal intensity of both the bleaching and IA. The synchronous oscillation for the bleaching and IA is, therefore, interpreted by the modulation of the transition dipole moment. Next we shall focus on the origin of the modulation in the Q-transition. Although the Q-transition is originally forbidden because of the symmetry of the electronic structure, the transition becomes allowed by mixing with the B-transition due to the configuration interaction and vibronic coupling.[9] Therefore, the additional intensity borrowing from the B-band accounts for the modulation of the Q-transition.

Evaluation of the Modulation of the Transition Dipole Moment. The additional mixing between the Q- and B-transition is induced by the pump pulse through the 244 cm^{-1} ruffling mode, and the degree of the mixing is enhanced or reduced depending on the phase of the vibrational motion of the TPPS molecules which compose a J-aggregate. Such is an outline of the dynamic intensity borrowing (DIB). DIB results in the transfer of the oscillator strength from the intense B-transition to the weak Q-transition. First, the amount of the modulation of the transition dipole moment is evaluated. The normalized modulation of the transition dipole moment of the molecule is expressed as $\delta\mu/\mu$, in which μ represents the Q-transition dipole moment of a TPPS molecule and $\delta\mu$ denotes the change of μ induced by the molecular vibration. Here it must be noticed that the modulation of μ also changes the intermolecular dipole−dipole interaction, J, which is given by

$$J = \mu^2(1 - 3\cos^2\theta)/\hbar a^3 \tag{1}$$

Here all transition dipoles in the TPPS molecules composing a J-aggregate are assumed to be parallel and making an angle θ with the aggregate axis. The molecules are equidistant with lattice constant a. Since the transition energy from the ground state to the first excited state of the aggregate is originally red-shifted by $2J$ in comparison with that of the monomer, the modulation of J gives rise to a peak shift of the J-band in the absorption spectrum. The amount of $\delta\mu$ and $\delta(2J)$ is estimated as follows. The induced absorption spectrum $\Delta A(\omega)$ is assumed to be modulated as $\Delta A'(\omega)$ by $\delta\mu$ and $\delta(2J)$, which is given by

$$\Delta A'(\omega) = \Delta A(\omega+\delta\omega(t))(1 + \delta u(t)) \tag{2}$$

where

$$\delta u(t) = (\delta(\Delta A)/\Delta A)\cos(\Omega t) = \delta(\mu^2)/\mu^2\cos(\Omega t) \tag{3}$$

$$\delta\omega(t) = \delta\omega\cos(\Omega t) = \delta(2J)\cos(\Omega t) \tag{4}$$

Here δu and $\delta\omega$ correspond to the amplitude modulation and the spectral shift of the signal, respectively. The modulation frequency, Ω, corresponds to the molecular vibration (244 cm^{-1}). Both δu and $\delta\omega$ are assumed to be independent of ω. Note that δu and $\delta\omega$ correspond to $\delta\mu^2/\mu^2$ and $\delta(2J)$, respectively. Equation 2 is approximately expressed as

$$\Delta A'(\omega) \cong \Delta A(\omega) + \left(\delta u\,\Delta A(\omega) + \delta\omega\frac{d\Delta A(\omega)}{d\omega}\right)\cos(\Omega t) \equiv \Delta A(\omega) + \Delta A_{osc}(\omega)\cos(\Omega t) \tag{5}$$

Since the experimentally obtained transmittance change is composed of the slow-dynamics component ($\Delta A(\omega)$) and the oscillating component ($\Delta A_{osc}(\omega)$), the former and the latter correspond to the first and second terms, respectively, in eq 5. To evaluate the slow-dynamics component, we performed a multichannel pump−probe measurement. The continuous spectrum of $\Delta A(\omega)$ at 20 fs delay time is depicted in Figure 8, which is measured by a polychromator and a CCD camera with sub-10-fs resolution. The signal amplitude of the continuous spectrum in Figure 8 is scaled down by a factor of 0.59 because of the different concentration of the J-aggregates. The slow-dynamics component, $\Delta A(\omega)$, can be approximately evaluated using the continuous induced absorption spectra. Assuming that $\Delta T/T(\omega)$ is proportional to $\Delta A(\omega)$ in the weak signal approximation, the oscillating component is fitted by both $\Delta A(\omega)$ and $d\Delta A(\omega)/d\omega$. As a result, we obtained $\delta u = (2.7 \pm 0.6) \times 10^{-2}$ and $\delta\omega = (5.6 \pm 1.3) \times 10^{-4}$ eV. Figure 8 shows the results of the fitting for $\Delta A_{osc}(\omega)$ and $\Delta A(\omega)$. The value of $\delta\mu/\mu$ is derived from δu and has the value

$$\frac{\delta\mu}{\mu} = \frac{\delta(\mu^2)}{2\mu^2} = \delta u/2 = 1.4 \pm 0.3\% \tag{6}$$

On the other hand, the ratio of the frequency shift $\delta\omega$ ($=\delta(2J)$) to $2J$ is determined to be $\delta\omega/2J = 0.3 \pm 0.1\%$ assuming $2J \sim 170$ meV from the stationary absorption spectrum. From eq 1, the modulation of $2J$ can be derived as follows:

$$\frac{\delta\omega}{2J} \equiv \frac{\delta(2J)}{2J} = \frac{2}{\mu}\delta\mu - \frac{3\sin 2\theta}{3\cos^2\theta - 1}\delta\theta - \frac{3}{a}\delta a \tag{7}$$

Since $\delta\mu/\mu$ and $\delta(2J)/2J$ are estimated to 1.4% and 0.3%, respectively, not only the modulation due to $\delta\mu$ but also the modulations due to $\delta\theta$ and δa should be taken into account. In

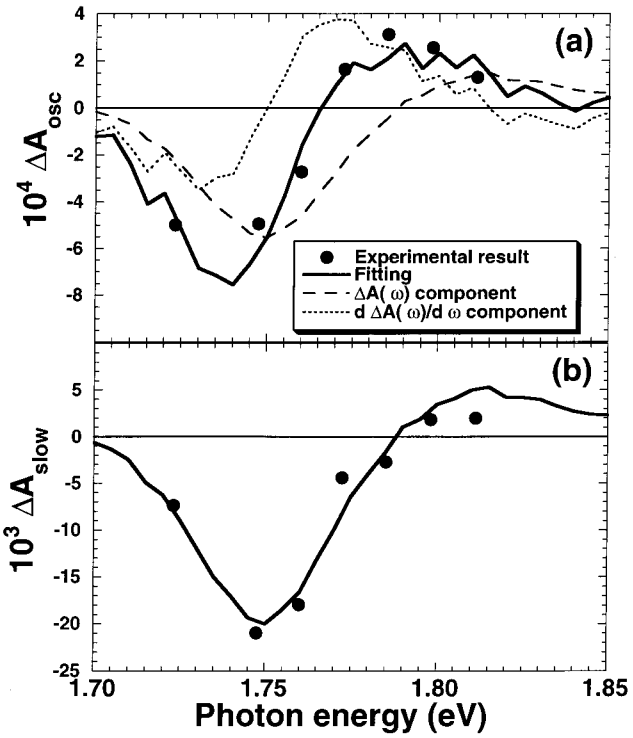

Figure 8. Results of the fitting for the oscillating component, $\Delta A_{osc}(\omega)$ (a), and slow-dynamics component, $\Delta A(\omega)$ (b), using eq 5. The continuous spectrum, $\Delta A(\omega)$, indicates the induced absorption spectrum detected by the multichannel pump−probe experiment. The oscillating component is fitted by $\Delta A(\omega)$ and $d\Delta A(\omega)/d\omega$.

this model, it is assumed that all μ and J are effectively modulated. A simulation which takes into account a local disorder effect is now under progress.

Dynamic Intensity Borrowing. In this subsection, the amount of the DIB is estimated. As was discussed, the weak oscillator strength of the Q-band is caused by the mixing with the B-band due to electron−electron correlation (configuration interaction) and vibronic coupling. We consider that the modulation of the transition dipole moment originates from DIB due to vibronic interaction between the Q- and B-transitions, which is induced by the pump pulse through the molecular vibration. Based on the vibronic coupling theory, a following calculation is performed to estimate the amount of the oscillator strength transfer from the B-band to the Q-band. Although the symmetry is important for the vibronic coupling mechanism, the symmetry of the 244 cm^{-1} ruffling mode is not clearly defined. The perturbed transition dipole moment between the Q-band and the ground state, $\mu' \equiv \mu + \delta\mu$, is expressed as follows in the first order using vibronic coupling theory:

$$\mu' = \mu + \delta\mu = \mu + \frac{H_{vib}}{E_B^0 - E_Q^0}\mu_B \qquad (8)$$

Here μ_B, E_B^0, E_Q^0, and H_{vib} denote the transition dipole moment due to the B-transition, the transition energies due to the B- and Q-transitions without the perturbation by the ruffling mode, and the perturbation to the Hamiltonian, respectively. The normalized value of the modulation of μ is given by

$$\frac{\delta\mu}{\mu} = \frac{H_{vib}}{E_B^0 - E_Q^0}\frac{\mu_B}{\mu} \qquad (9)$$

$E_B^0 - E_Q^0 \sim 0.94$ eV and $\mu_B/\mu \sim 2.6$ are estimated from the stationary absorption spectrum of the monomer. The amount of $\delta\mu/\mu$ is calculated in the previous subsection as $\delta\mu/\mu = 1.4\%$. By substituting these coefficients, $H_{vib} = 5.4$ meV $= 41$ cm^{-1} is obtained, which is much less than the vibration frequency, 244 cm^{-1}. The modulated transition dipole moment is also estimated as $\mu' = \mu + (5.4 \times 10^{-3})\mu_B$. A similar intensity borrowing mechanism has been discussed in the stationary resonance Raman spectrum of metalloporphyrins.[40−42] The resonance Raman spectra under the B- and Q-band excitations show dominant contributions of the Albrecht A-term and the B-term scattering, respectively. The dominant contribution of the B-term under the resonant Q-excitation is also explained by the intensity borrowing mechanism from the B-band to the Q-band.

Conclusion

The coherent molecular vibration coupled to the Frenkel exciton is observed using a sub-5-fs pulse. The oscillation in the time trace originates from the molecular vibration and is assigned to the 244 cm^{-1} ruffling mode. It is interpreted by the modulated transition dipole moment of the Q-band, which is due to the dynamic intensity borrowing (DIB) mechanism from the intense B-transition to the weak Q-transition through the molecular vibration. The amount of the modulation is estimated to be $\delta\mu/\mu = 1.4\%$. The DIB is a new mechanism of ultrafast nonlinearity and is observed for the first time in the present study.

Acknowledgment. The authors thank Drs. H. F. Hofmann and T. Fuji for enlightening discussions. The authors gratefully acknowledge helpful advice by Dr. A. Shirakawa of the University of Electro-communications on experimental techniques. Thanks are due to Dr. Y. Takasu and Prof. I. Nishio of Aoyama Gauin University for Raman scattering measurements. The authors appreciate Dr. S. Abe of Electrotechnical Laboratory for stimulating discussion. The work is partly supported by Research for the Future of Japan Society for the Promotion of Science (JSPS-RFTF-97P-00101).

References and Notes

(1) *J-aggregates*; Kobayashi, T., Ed.; World Scientific: River Edge, NJ, 1996.
(2) Mukamel, S. *Principles of Nonlinear Optical Spectroscopy*; Oxford: New York, 1995.
(3) Davydov, A. S. *Theory of Molecular Excitons*; Plenum: New York, 1971.
(4) Kobayashi, T. *Mol. Cryst. Liq. Cryst.* **1998**, *314*, 1−11.
(5) Jelly, E. E. *Nature* **1936**, *138*, 1009−1010.
(6) Sheibe, G. *Angew. Chem.* **1936**, *49*, 563−564.
(7) Fleisher, E. B.; Palmer, J. M.; Srivastava, T. S.; Chatterjee, A. *J. Am. Chem. Soc.* **1971**, *93*, 3162−3167.
(8) Pasternack, R. F.; Huber, P. R.; Boyd, P.; Engasser, G.; Francesconi, L.; Gibbs, E.; Fasella, P.; Venturo, G. C.; Hinds, L. de C. *J. Am. Chem. Soc.* **1972**, *94*, 4511−4517.
(9) Dolphin, D., Ed.; *The Porphyrins, Volume III, Physical Chemistry, Part A*; Academic Press: New York, 1979.
(10) Barber, D.; Fretag-Beeston, R. A.; Whitten, D. G. *J. Phys. Chem.* **1991**, *95*, 4074−4086.
(11) Ohno, O.; Kaizu, Y.; Kobayashi, H. *J. Chem. Phys.* **1993**, *99*, 4128−4139.
(12) Shick, G. A.; O'Grady, M. R.; Tiwari, R. K. *J. Chem. Phys.* **1993**, *97*, 1339−1345.
(13) Ribo, J. M.; Crusats, J.; Farrera, J. A.; Valero, M. L. *J. Chem. Soc., Chem. Commun.* **1994**, 681−682.
(14) Akins, D. L.; Ozcelik, S.; Zhu, H. R.; Guo, C. *J. Phys. Chem.* **1996**, *100*, 14390−14396.
(15) Chan, I. Y.; Hallock, A. J. *J. Chem. Phys.* **1997**, *107*, 9297−9301.
(16) Maiti, N. C.; Mazumdar, S.; Periasamy, N. J. *J. Phys. Chem.* **1998**, *102*, 1528−1538.
(17) Misawa, K.; Kobayashi, T. *J. Chem. Phys.* **1999**, *110*, 5844−5850.
(18) Scherer, P. O. J.; Knapp, E. W.; Fischer, S. F. *Chem. Phys. Lett.* **1984**, *106*, 191−196.

(19) Knapp, E. W.; Scherer, P. O. J.; Fischer, S. F. *Chem. Phys. Lett.* **1984**, *111*, 481−486.
(20) Spano, F. C.; Kuklinski, J. R.; Mukamel, S. *Phys. Rev. Lett.* **1990**, *65*, 211−214.
(21) Chachisvilis, M.; Pullerits, T.; Jones, M. R.; Hunter, C. N.; Sundstrom, V. *Chem. Phys. Lett.* **1994**, *224*, 345−351.
(22) Fragnito, H. L.; Bigot, J. Y.; Becker, P. C.; Shank, C. V. *Chem. Phys. Lett.* **1989**, *160*, 101−104.
(23) Pollard, W. T.; Fragnito, H. L.; Bigot, J. Y.; Shank, C. V.; Mathies, R. A. *Chem. Phys. Lett.* **1990**, *168*, 239−245.
(24) Pollard, W. T.; Dexheimer, S. L.; Wang, Q.; Peteanu, L. A.; Shank, C. V.; Mathies, R. A. *J. Phys. Chem.* **1992**, *96*, 6147−6158.
(25) Zhu, L. Y.; Sage, J. T.; Champion, P. M. *Science* **1994**, *266*, 629−632.
(26) Yeh, A. T.; Cerullo, G.; Banin, U.; Mews, A.; Alivisatos, A. P.; Shank, C. V. *Phys. Rev. B* **1999**, *59*, 4973−4979.
(27) Cerullo, G.; Lanzani, G.; Muccini, M.; Taliani, C.; Silvestri, S. D. *Phys. Rev. Lett.* **1999**, *83*, 231−234.
(28) Kobayashi, T.; Shirakawa, A. *Chem. Phys. Lett.* **2000**, *321*, 385−393.
(29) Takeuchi, S.; Tahara, T. *Chem. Phys. Lett.* **2000**, *326*, 430−438.
(30) Kobayashi, T.; Shirakawa, A. *Appl. Phys. B* **2000**, *70*, S239−S246.
(31) Fuji, T.; Saito, T.; Kobayashi, T *Chem. Phys. Lett.*, in press.
(32) Shirakawa, A.; Sakane, I.; Takasaka, M.; Kobayashi, T. *Appl. Phys. Lett.* **1999**, *74*, 2268−2270.
(33) Misawa, K.; Ono, H.; Minoshima, K.; Kobayashi, T. *Appl. Phys. Lett.* **1993**, *63*, 577.
(34) Brito-Cruz, H.; Gordon, J. P.; Becker, P. C.; Fork, R. L.; Shank, C. V. *IEEE J. Quantum Electron.* **1988**, *24*, 261−266.
(35) Tokunaga, E.; Terasaki, A.; Kobayashi, T. *J. Opt. Soc. Am. B* **1995**, *12*, 753−771.
(36) Spano, F. C. *Phys. Rev. Lett.* **1991**, *67*, 3424−3427.
(37) Knoester, J. *Phys. Rev. A* **1993**, *47*, 2083−2098.
(38) Minoshima, K.; Taiji, M.; Misawa, K.; Kobayashi, T. *Chem. Phys. Lett.* **1994**, *218*, 67−72.
(39) Kano, H.; Kobayashi, T. *Technical Digest of Quantum Electronics and Laser Science Conference 99*; 1999, p 10.
(40) Li, X.-Y.; Czernuszewicz, R. S.; Kincaid, J. R.; Spiro, T. G. *J. Am. Chem. Soc.* **1989**, *111*, 7012−7023.
(41) Czernuszewicz, R. S.; Li, X.-Y.; Spiro, T. G. *J. Am. Chem. Soc.* **1989**, *111*, 7024−7031.
(42) Schweitzer-Stenner, R.; Stichternath, A.; Dreybrodt, W.; Jentzen, W.; Song, X.-Z.; Shelnutt, J. A.; Nielsen, O. F.; Medforth, C. J.; Smith, K. M. *J. Chem. Phys.* **1997**, *107*, 1794−1815.